J Fluoresc (2012) 22:899–906
DOI 10.1007/s10895-011-1028-7

ORIGINAL PAPER

Influence of Catalyses on the Preparation of $YVO_4:Eu^{3+}$ Phosphors by the Sol–gel Methodology

Michelle Saltarelli · Priscilla P. Luz · Marcela G. Matos · Emerson H. de Faria · Katia J. Ciuffi · Paulo S. Calefi · Lucas A. Rocha · Eduardo J. Nassar

Received: 16 October 2011 / Accepted: 19 December 2011 / Published online: 30 December 2011

Abstract $YVO_4:Eu^{3+}$ phosphors have been prepared by the hydrolytic sol–gel methodology, with and without alkaline catalyst. The solid powder was obtained by reaction between yttrium III chloride and vanadium alkoxides; the europium III chloride was used as structural probe. The powder was treated at 100, 400, 600, or 800 °C for 4 h. The samples were characterized by X-ray diffraction, thermal analysis, and photoluminescence. The XRD patterns revealed YVO_4 crystalline phase formation for the sample prepared without the catalyst and heat-treated at 600 °C and for the sample prepared in the presence of ammonium as catalyst and heat-treated at 100 °C. The average nanosized crystallites were estimated by the Scherrer equation. The sample which was produced via alkaline catalysis underwent weight loss in two stages, at 100 and 400 °C, whereas the sample obtained without catalyst presented four stages of weight loss, at 150, 250, 400, and 650 °C. The excitation spectra of the samples treated at different temperatures displayed the charge transfer band (CTB) at 320 nm. PL data of all the samples revealed the characteristic transition bands arising from the $^5D_0 \rightarrow {}^5F_J$ (J=0, 1, 2, 3, and 4) manifolds under maximum excitation at 320, 394, and 466 nm in all cases. The $^5D_0 \rightarrow {}^7F_2$ transition often dominates the emission spectra, indicating that the Eu^{3+} ion occupies a site without inversion center. The long lifetime suggests that the matrix can be applied as phosphors. In conclusion, the sol–gel methodology is a very efficient approach for the production of phosphors at low temperature.

M. Saltarelli · P. P. Luz · M. G. Matos · E. H. de Faria · K. J. Ciuffi · P. S. Calefi · L. A. Rocha · E. J. Nassar (✉)
Universidade de Franca,
Av. Dr. Armando Salles Oliveira, 201 Pq. Universitário,
CEP 14.404-600, Franca, SP, Brazil
e-mail: ejnassar@unifran.br

Keywords Lifetime · Nanosize crystallites · Europium III · Phosphors

Introduction

The sol–gel methodology has been employed for the synthesis of a wide variety of materials at low temperature, the formation of a polymer network depending on the precursors and reaction conditions [1–5]. Several materials can be obtained by using either the hydrolytic or the non-hydrolytic sol–gel route, such as hybrid materials, phosphors, films, mesoporous materials, composites, nanoparticles, glasses, coating, waveguides, and biomaterials, among others [6–18].

The sol–gel methodology offers many advantages, like low temperature and pressure [19]. Moreover, it can be used to prepare the yttrium orthovanadate (YVO_4) matrix doped with lanthanide ions, which can be applied in lamps, lasers, TV phosphors, and plasma display panel (PDP) phosphors [20]. The YVO_4 matrix is an important optical material due to its thermal, mechanical, and optical properties, which allows for its use in countless devices. Doping of this matrix with Eu^{3+} has afforded materials that have been utilized as red phosphors in color television and cathode ray tubes (CRTs) owing to their high luminescence efficiency upon electron beam excitation [21]. Indeed, there are many efficient methods that furnish this matrix. For instance, the household microwave oven has been employed in the preparation of an oxide mixture that was irradiated at 840 °C for 150 s [20, 22]. Juan Wang et al. and Fei He et al. [21, 23] have used the hydrothermal synthesis to obtain the YVO_4 matrix with an autoclave operating at 180 °C for 24 h. Spray pyrolysis is another technique that has been utilized for the synthesis of this matrix [24], and the precursors obtained by spray pyrolysis were treated from 300 °C to 1,200 °C for 4 h.

Xue-Qing Su and Bing Yan [25, 26] have synthesized the matrix by the co-precipitation methodology using a temperature of 1,100 °C. The Pechini process has been employed by Yee-Shin Chang et al. in the preparation of the YVO_4 matrix at a temperature of 800 °C [27]. In the conventional synthetic process, YVO_4 has been prepared by the solid-state process at a temperature above 1,000 °C [28].

Comparison between the sol–gel process and other methodologies has shown that most of the synthetic methods require high temperatures for the achievement of short reaction times, whereas the use of low temperatures demands long reactions. In contrast, the sol–gel route calls for low reaction temperature and short time periods for the preparation of the final material.

In this work the YVO_4 matrix doped with Eu^{3+} ions has been prepared by the conventional sol–gel methodology using alkoxides as precursors. The influence of the catalyst on matrix formation has also been investigated. The obtained materials have been characterized and their properties have been estimated by X-ray diffraction (XRD), thermal analysis (TA), and photoluminescence (PL).

Experimental

Preparation of the YVO_4:Eu^{3+} Powder

$EuCl_3$ and YCl_3 were prepared after calcination of the corresponding oxides (Eu_2O_3 and Y_2O_3 – Aldrich) for 2 h at 900 °C. The oxides were dissolved in HCl 6 mol.L^{-1} (Merk). Excess HCl and H_2O were evaporated. Ethanol was then added and evaporated three times. The final concentration of the rare earth (RE) ion in the ethanolic solution was 0.1 mol L^{-1}.

The YVO_4:Eu^{3+} matrix was obtained by means of the modified hydrolytic sol–gel methodology. To this end, ethanolic solutions of YCl_3 (41.00 mL) and $EuCl_3$ (0.410 mL) were added to the solution of isopropylic alcohol and water under stirring, followed by addition of vanadium isopropoxide (0.966 mL) at a V/Y molar ratio of 1:1 (V:Y). The beta-diketone (acetylacetonate) was added as an alkoxide stabilizer. The reaction was left under magnetic stirring for 48 h at room temperature. After this period, the solvent was evaporated. The solid was then washed, dried at 100 °C, and further treated at 400, 600, or 800 °C for 4 h.

The samples were designated S1C (prepared in the presence of ammonium catalyst) and S1S (without catalyst).

Characterization

Thermal analysis (TG/DTA/DSC) was carried out on the Thermal Analyst 2100 – TA Instruments SDT 2960 simultaneous DTA-TG in nitrogen atmosphere, at a heating rate of 20 °C/min, from 25 °C to 900 °C.

The X-ray diffraction (XRD) measurements were performed at room temperature using a Rigaku Geigerflex D/max-c diffractometer with monochromated CuK_α radiation (λ=1.5405 Å). Diffractograms were recorded in the 2θ range from 4° to 80° at a resolution of 0.05°.

Photoluminescence (PL) data were obtained under continuous Xe lamp (450 W) excitation with a spectrofluometer SPEX – Fluorolog II, at room temperature. The emission was collected at 90° from the excitation beam. The slits were placed at 1.0 and 0.2 mm for excitation and emission, respectively, giving a bandwidth of 3.5 and 0.5 nm. Oriel 58916 (exc.) and Corning 97612 (em.) filters were used.

Results and Discussion

Thermal Analysis (TG/DTA/DSC)

Figures 1a and b show the TG/DTG curves recorded for the powders obtained by means of the sol–gel hydrolytic

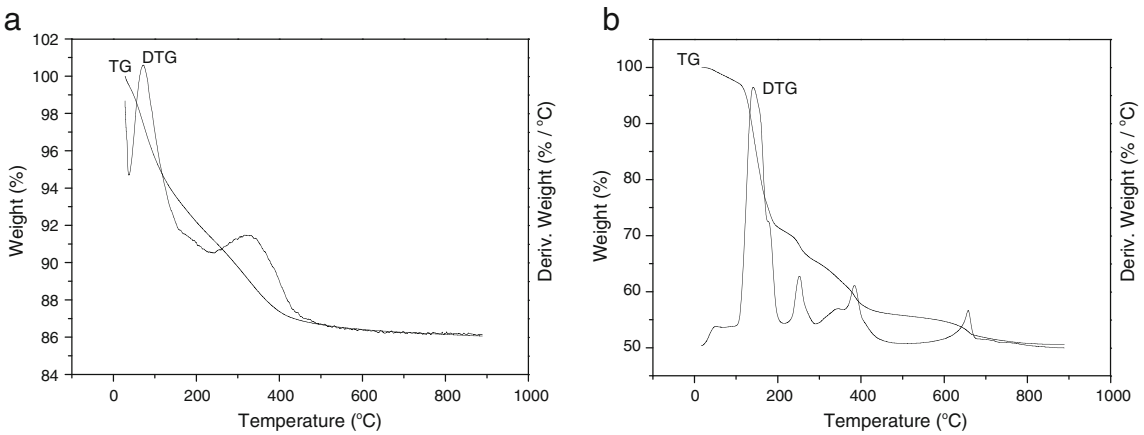

Fig. 1 TG/DTG curves for the YVO_4:Eu^{3+} matrix prepared in the presence (**a**) and in the absence (**b**) of the catalyst, followed by drying at 100 °C

methodology carried out in the presence (S1C) or in the absence (S1S) of a catalyst, followed by drying at 100 °C.

The TG/DTG curves reveal peaks accompanied by mass losses at 73 °C for the sample synthesized in the presence of the catalyst. This can be attributed to the loss of water molecules weakly bound to the oxide and solvent molecules. Another mass loss appears at 329 °C, ascribed to pyrolysis of organic matter remaining from the synthesis. The end of the mass loss occurs after 500 °C, with a total loss of 14%.

The sample prepared in the absence of the catalyst presents four stages of mass loss, with peaks at 141, 252, 384, and 657 °C, which can be assigned to the loss of water molecules, solvent molecules, pyrolysis of organic matter remaining from the synthesis, and structural arrangement, respectively. The mass loss can be accompanied by reaction between precursors, which can be better visualized in the X ray-diffraction pattern. The total mass loss was 48% (w/w).

X-Ray Diffraction (XRD)

Figure 2 depicts the XRD patterns of the S1C powder obtained after treatment at 100, 400, 600, or 800 °C for 4 h.

The XRD patterns give evidence of the formation of YVO_4 phases at 100, 400, 600, and 800 °C, as indicated by the peaks at 2θ = 18, 25, 33, and 49°, which correspond to card 17–341 wakefieldite (Y) and can be indexed to the tetragonal phase. Table 1 lists the peaks and their relative intensities for the card and samples.

From the data presented in Table 1 it can be seen that the XRD pattern of the S1C samples prepared by the modified hydrolytic sol–gel process and treated at different temperatures contains several peaks that are ascribed to the YVO_4 matrix. The samples treated at 100 and 400 °C display broad peaks, which indicate formation of the matrix. The crystallization of the materials becomes evident with increasing heat-treatment temperatures. An amorphous phase disappears in the case of the powders treated at 800 °C, and the relative intensity shown in Table 1 reveals formation of the YVO_4 phases. The peaks related to yttrium and vanadium oxide are not observed, which is an indication that the precursors reacted completely. In the literature there are numerous works reporting on different methodologies for the preparation of the YVO_4 matrix [20, 28], but the temperature employed in these procedures is always higher than the one used in the present work. Indeed, with the technique

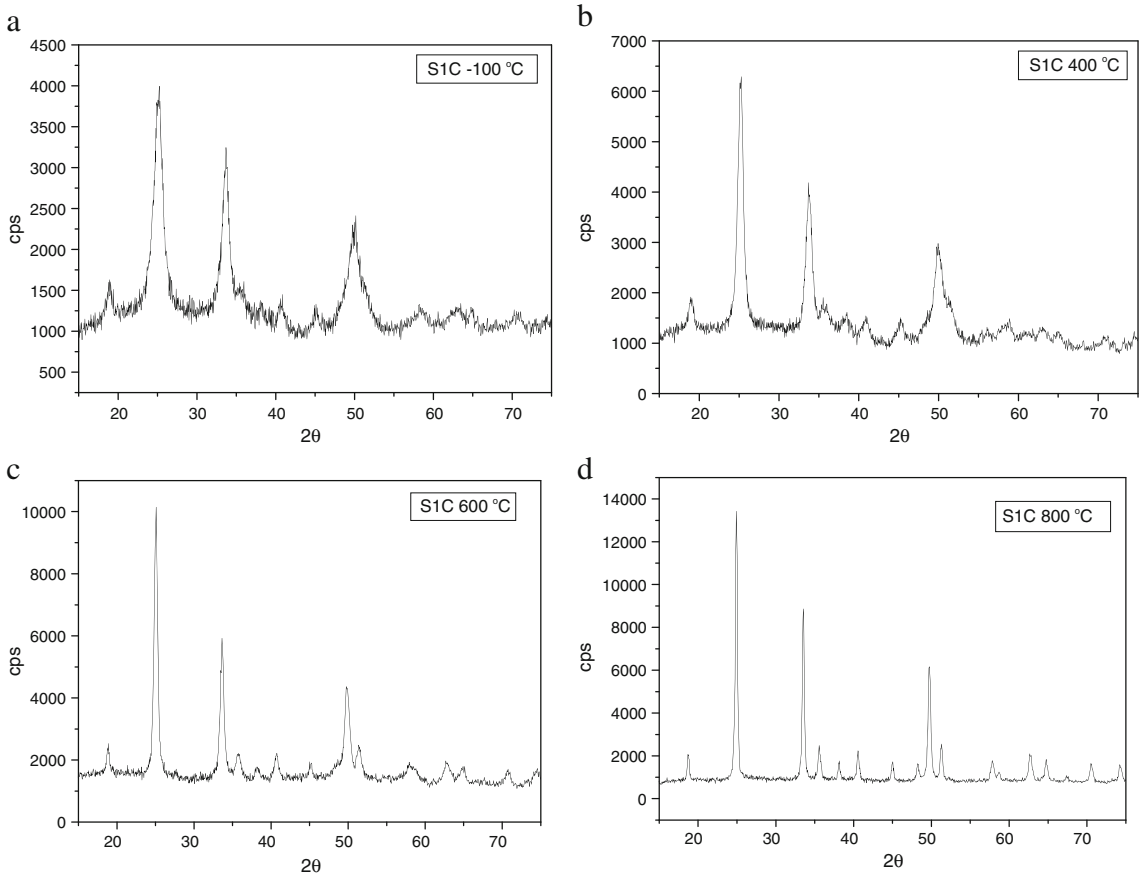

Fig. 2 X-Ray diffraction patterns of the YVO_4:Eu^{3+} matrix prepared in the presence of the catalyst and treated at (**a**) 100, (**b**) 400, (**c**) 600, or (**d**) 800 °C

Table 1 Peaks and relative intensity for the standard and the S1C samples treated at different temperatures

Sample	2θ			
Card 17–341	18.86 (10%)	25.05 (100%)	33.64 (45%)	49.79 (40%)
S1C-100 °C	18.82 (40%)	25.09 (100%)	33.57 (80%)	50.08 (60%)
S1C-400 °C	18.92 (30%)	25.17 (100%)	33.69 (65%)	49.94 (47%)
S1C-600 °C	18.98 (25%)	25.04 (100%)	33.69 (58%)	49.86 (42%)
S1C-800 °C	18.63 (15%)	25.01 (100%)	33.59 (66%)	49.66 (46%)

utilized herein formation of the YVO_4 phases was found to begin at 100 °C for the S1C samples (Fig. 3).

Table 2 summarizes the peaks and their relative intensity for the card and samples.

The XRD pattern of the S1S samples, prepared without catalyst, reveals the presence of several peaks and amorphous phases for the samples treated at 100 °C (S1S-100 °C) and 400 °C (S1S-400 °C). The S1S-100 °C sample probably consists of a mixture of the oxide precursors. As for S1S-400 °C, the peaks in 2θ = 25 and 33º suggest that formation of the YVO_4 matrix is taking place. Concerning S1S-600 °C and S1S-800 °C, the peaks in 2θ = 18, 25, 33, and 49º are attributed to the YVO_4 matrix (card 17–341), clearly showing that the latter are crystalline materials. In addition, the peaks related to yttrium and vanadium oxide are not detected in the case of the samples treated at higher temperatures. Compared with the S1C samples, it is thus clear that the presence of the basic catalyst favors formation of the crystalline phase at lower temperatures (100 and 600 °C for the S1C and S1S samples, respectively). However, the S1S materials are more crystalline, as judged from the width of the XRD peaks.

The crystallite size can be estimated by the Scherrer equation Eq. 1 using the peak broadening of the XRD reflection [29]:

$$L = K\lambda/\beta \cos\theta, \quad (1)$$

where L denotes the average crystallite size, λ represents the wavelength of the X-ray radiation (λ=0.154056 nm), and K

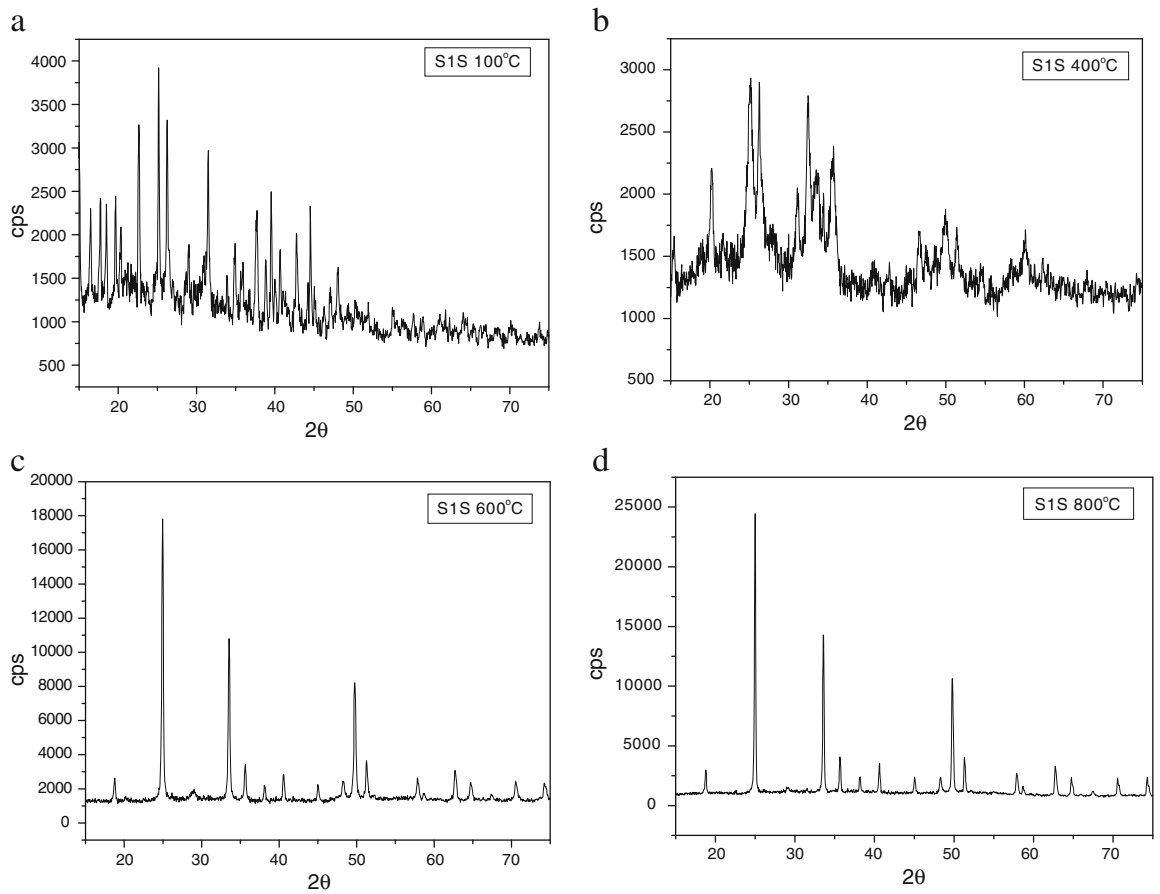

Fig. 3 X-Ray diffraction patterns of the $YVO_4:Eu^{3+}$ matrix prepared in the absence of catalyst and treated at (**a**) 100, (**b**) 400, (**c**) 600, or (**d**) 800 °C

Table 2 Peaks and relative intensity for the standard and the S1S samples treated at different temperatures

Sample	2θ			
Card 17–341	18.86 (10%)	25.05 (100%)	33.64 (45%)	49.79 (40%)
S1S-100 °C	–	–	–	–
S1S-400 °C	–	25.17 (100%)	32.65 (94%)	–
S1S-600 °C	18.74 (14%)	24.90 (100%)	33.60 (60%)	49.77 (46%)
S1S-800 °C	18.69 (12%)	25.10 (100%)	33.52 (59%)	49.81 (43%)

is a constant related to the shape of the crystallite and is approximately equal to unity. β, which is experimentally measured, is the full width of the peak at half of the maximum intensity (rad) and is expressed in its squared form as a squared sum function of the two main contributions, according to Eq. 2 depicted below. In the latter equation, β_1 represents the contribution of the crystallite size to the peak broadening, while β_2 is the instrumental broadening contribution.

$$\beta = \beta_1{}^2 + \beta_2{}^2 \quad (2)$$

On the basis of the XRD data, Table 3 displays the average nanosized crystallites that were produced during the synthesis of the YVO_4 matrix by the modified sol–gel methodology.

Photoluminescence (PL)

Figure 4 depicts the excitation spectra of Eu^{3+} ion-doped YVO_4 host samples monitored at the $^5D_0 \rightarrow {}^7F_2$ transition.

The excitation spectra of the samples were recorded by fixing the emission wavelength at the Eu^{3+}: $^5D_0 \rightarrow {}^7F_2$ transition. The bands can be assigned to different excitation processes. The sharp lines observed in the 350–475 nm range (*f-f* transitions) are attributed to transitions from the $^7F_0$ level. The PL spectra of the powders display a broad band located around 320 nm, which corresponds to the absorption by the YVO_4 host crystal [30].

The Eu^{3+}-O^{2-} charge transfer to the broad band can take place below 350 nm, but the several publications concerning YVO_4:Eu materials have assigned this band to $VO_4{}^{3-}$ rather than to the Eu^{3+}-O^{2-} charge transfer band [31, 32]. This is because in YVO_4:Eu the V^{5+}-O^{2-} charge transfer relative to $VO_4{}^{3-}$ occurs much more easily than the one related to Eu^{3+}-O^{2-} in view of the large differences of charges and ionic radii between V^{5+} (r=0.0355 nm) and Eu^{3+} (r=0.107 nm) [24]. Table 4 presents the maximum absorption band in the excitation spectra registered for the samples prepared in this work.

The samples prepared in the presence of the catalyst presented bands at 316 nm, for the sample treated at 400 °C, and 320 nm, in the case of the samples treated at 600 and 800 °C.

The excitation spectra for the samples prepared in the presence of the catalyst revealed that the sample treated at 400 °C exhibited a band at 316 nm, while the ones treated at 600 and 800 °C shifted to 320 nm. With respect to the samples synthesized in the absence of the catalyst, there was an increase in the excitation wavelength of this broad band with rising heat-treatment temperature, namely 302, 312, and 324 nm for the samples heated at 400, 600, and 800 °C, respectively. These wavelengths agree with the change in the symmetry of the ion. In crystalline YVO_4, the T_d symmetry of $VO_4{}^{3-}$ (free ion) is reduced to D_{2d} by the crystal field, which causes a splitting of the degenerate energy levels of $VO_4{}^{3-}$; the bands at 302 and 320 nm correspond to electric or magnetic dipole-allowed transitions from the $^1A_2(^1T_1)$ ground state to the $^1A_1(^1E)$ and $^1B_1(^1E)$ excited states of the $VO_4{}^{3-}$ ion, respectively [31].

The shift in the wavelength can be due to lattice distortions, because in smaller particles the V-O average distances are longer as compared to larger particles. The order factor can be due to disorder, since the Eu^{3+} ions can be located on the surface of the annealed samples and therefore occupy the order lattice site therein [26, 33]. This can be confirmed by X-ray diffraction, crystallite size, and crystallinity of the samples at different heat-treatment temperatures.

Figure 5 illustrates the emission spectra of the Eu^{3+} ion in the YVO_4 host, monitored at the CTB.

Table 3 Average crystallite size for the S1C and S1S samples treated at different temperatures

	Samples							
	S1C-100	S1C-400	S1C-600	S1C-800	S1S-100	S1S-400	S1S-600	S1S-800
Crystal size (nm)	6	8	15	28	–	6	42	55

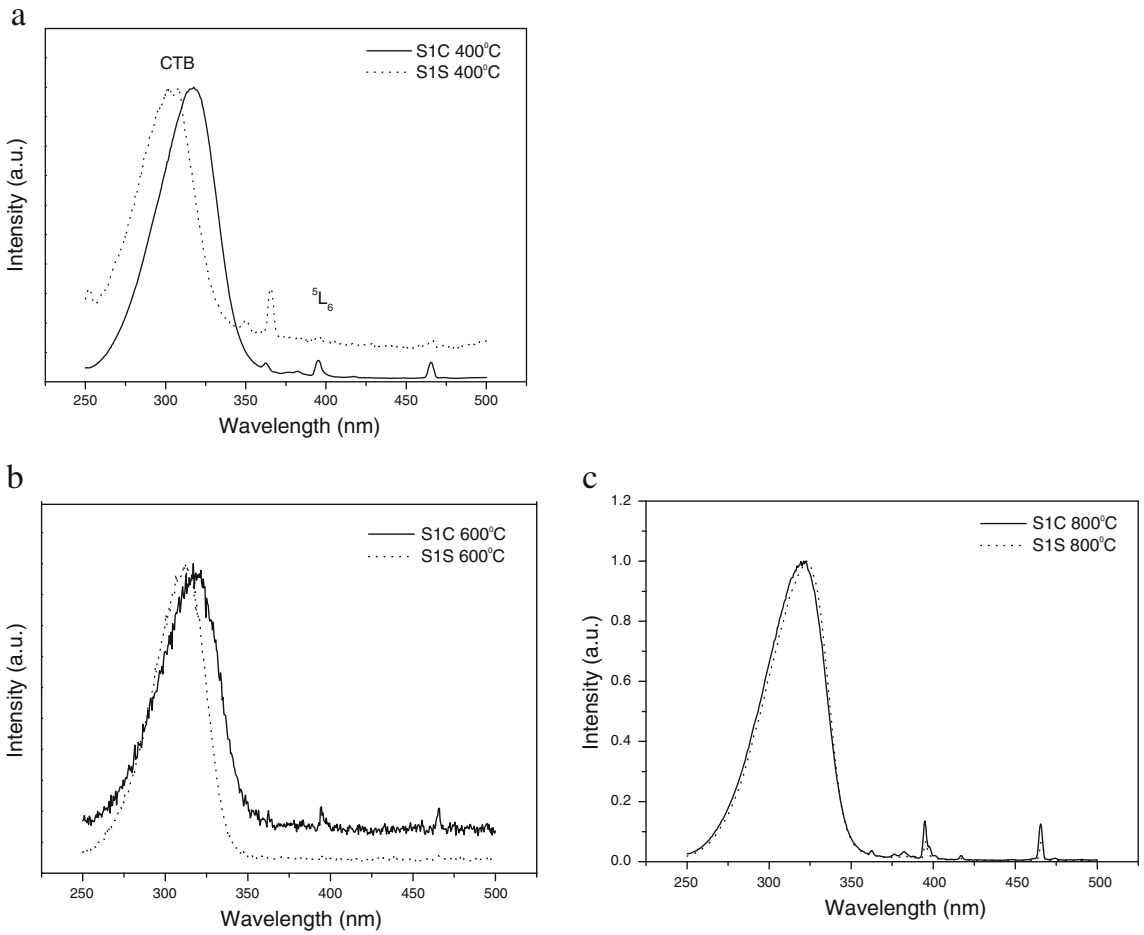

Fig. 4 Excitation spectra of the Eu^{3+} ion doped into the YVO_4 host treated at (**a**) 400, (**b**) 600, and (**c**) 800 °C for 4 h, $^5D_0 \rightarrow {}^7F_2$, λ_{em}=614 nm

The emission spectra of the Eu^{3+} ion in the YVO_4 host, obtained by excitation at the CTB and $^5L_6$ level, present the $^5D_0 \rightarrow {}^7F_J$ (J=0–4) emission lines of the ion dominated by the $^5D_0 \rightarrow {}^7F_2$ (~ 614 nm) electric dipole transition, which is strongly dependent on the Eu^{3+} surroundings. When the Eu^{3+} ion is situated in a low symmetry site (without inversion center), the hypersensitive transition $^5D_0 \rightarrow {}^7F_2$ is often dominating in the emission spectra. This indicates that the Eu^{3+} ion occupies a site without inversion center. The $^5D_0 \rightarrow {}^7F_1$ transition (591 nm) is purely magnetic-dipole allowed, and not restricted by any symmetry [34, 35]. This is in agreement with the D_{2d} symmetry, which has no inversion center.

The samples treated at 100 °C do not display a band in the emission spectra. This can be attributed to energy loss by vibration mechanisms involving water and solvent molecules.

The samples excited at the CTB give rise to more defined peaks as compared to the samples excited at the $^5L_6$ level. This is because the energy transfer is more efficient than the direct excitation of the ion.

The emission spectrum reveals the presence of not only the characteristic transition lines from the $^5D_0$ level, but also of the transitions from the $^5D_1$ and $^5D_2$ levels of the Eu^{3+} ion, which have very weak intensity. The presence of emission lines from higher excited states is ascribed to the low vibration energy of the VO_3^- groups (823 cm^{-1}) [24].

Table 5 lists the lifetime of the $^5D_0 \rightarrow {}^7F_2$ transition when the sample is excited at the CTB.

Table 4 Maximum excitation wavelength of the samples prepared herein

	Samples							
	S1C-100	S1C-400	S1C-600	S1C-800	S1S-100	S1S-400	S1S-600	S1S-800
λ (nm)	–	316	320	320	–	302	312	324

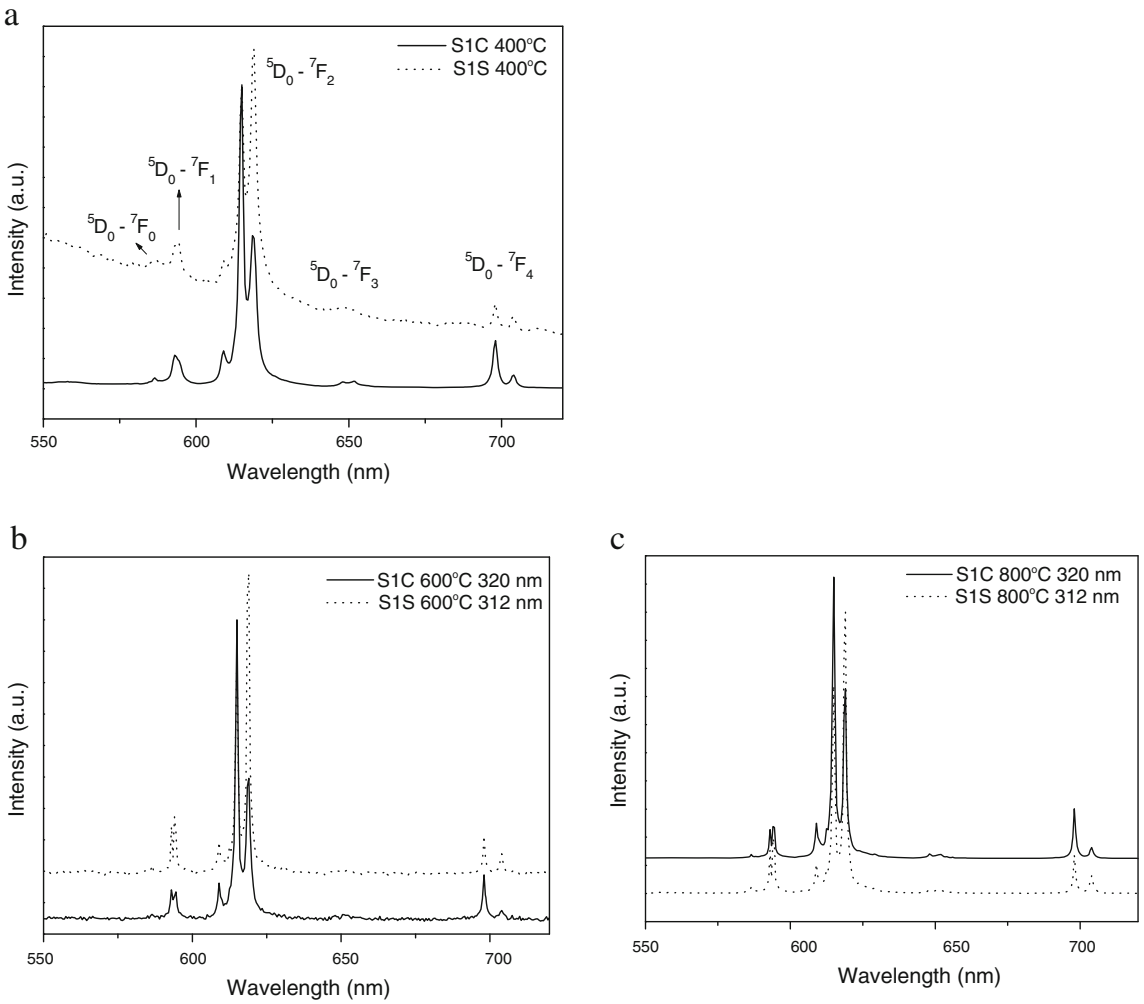

Fig. 5 Emission spectra of the Eu^{3+} ion in the S1C and S1S YVO_4 samples treated at (**a**) 400, (**b**) 600, and (**c**) 800 °C for 4 h and excited at the CTB

Only one lifetime was observed for the samples excited at the CTB. Excitation at this band thus demonstrated that energy transfer takes place in only one Eu^{3+} site. The increase in lifetime with rising heat-treatment temperature can be explained by reduction in the vibrational modes, which in turn promotes energy losses. All the samples prepared with catalyst displayed higher lifetime than the samples prepared without catalyst. The thermal analysis carried out for the samples prepared with and without catalyst showed that weight loss occurred up to 500 °C and around 800 °C, respectively. This can be due to precursor residues in the matrix, which can promote vibrational energy loss.

Conclusion

The preparation of YVO_4 doped with europium ion by the sol–gel route has been demonstrated. The YVO_4 phases were obtained at lower temperature than the ones traditionally employed for the synthesis of this matrix by other methodologies. In addition, different precursors were used in the present case. The crystal sizes and sample crystallinity depend on the heat-treatment temperature. The XRD study showed that the onset of phase formation took place at 100 °C for the S1C samples, and that only one phase was formed. The excitation spectra revealed that the energy of the charge

Table 5 Lifetime (τ) of the samples containing Eu^{3+} and excited at CTB → $^7F_2$. The S1C and S1S samples were annealed at 100, 400, 600, or 800 °C for 4 h

	Samples							
	S1C-100	S1C-400	S1C-600	S1C-800	S1S-100	S1S-400	S1S-600	S1S-800
τ (ms)	–	0.98	1.41	1.92	–	0.71	0.84	1.20

transfer bands depends on the symmetry of the Eu^{3+} ion site. The characteristic red emission of Eu^{3+} was observed in the photoluminescence measurements.

Acknowledgements The authors acknowledge FAPESP, CNPq, and CAPES (Brazilian research funding agencies) for support of this work and the Rare Earths laboratory of the University of São Paulo for the luminescence data.

References

1. Wright JD, Sommerdijk NAJM (2001) Sol–gel materials: chemistry and application. Taylor & Francis, London
2. Brinker CJ, Scherer GW (1990) Sol–gel science: the physics and chemistry of sol–gel processing. Academic Press, San Diego
3. Aegerter MA, Menning M (2004) Sol–gel technologies for glass producers and users. Kluwer Academic Publishers, Germany
4. Hench LL (1998) Sol–gel silica. Noyes Publications
5. Mark JE, Lee CYC, Bianconi PA (1995) Hybrid organic-inorganic composites. American Chemical Society, Washington DC
6. Sanchez C, de Soler-Illia GJDAA, Ribot F, Grosso D (2003) Design of functional nano-structured materials through the use of controlled hybrid organic–inorganic interfaces, Nanomaterials and their physical properties. CR Chimie 6:1131–1151
7. Mutin PH, Vioux A (2009) Nonhydrolytic processing of oxide-based materials: simple routes to control homogeneity, morphology, and nanostructure. Chem Mater 21:582–596
8. Gaponenko NV (2002) Synthesis and optical properties of films formed by the sol-gel method in mesoporous matrices. J Appl Spectrosc 69:1–20
9. Carlos LD, Ferreira RAS, Bermudez VZ, Ribeiro SJL (2001) Full-color phosphors from amine-functionalized crosslinked hybrids lacking metal activator ions. Adv Funct Mater 11:111–115
10. Rocha LA, Caiut JMA, Messaddeq Y, Ribeiro SJL, Martines MAU, Freiria JC, Dexpert-Ghys J, Verelst M (2010) Non-leachable highly luminescent ordered mesoporous SiO2 spherical particles. Nanotechnology 21:1–6
11. Bandeira LC, Ciuffi KJ, Calefi PS, Nassar EJ (2010) Silica matrix doped with calcium and phosphate by sol-gel. Adv Biosci Biotechnol 1:200–207
12. Petil O, Zanotto ED, Hench LL (2001) Highly bioactive P_2O_5-Na_2O-CaO-SiO_2 glass-ceramics. J Non-Cryst Solids 292:115–126
13. de Campos BM, Bandeira LC, Calefi PS, Ciuffi KJ, Nassar EJ, Silva JVL, Oliveira M, Maia IA (2011) Protective coating materials on nylon substrate by sol-gel. Virtual Phys Prototyp 6(1):33–39
14. Pereira PFS, Matos MG, Avila LR, Nassor ECO, Cestari A, Ciuffi KJ, Calefi PS, Nassar EJ (2010) Red, green and blue (RGB) emission doped $Y_3Al_5O_{12}$ (YAG) phosphors prepared by non-hydrolytic sol–gel route. J Lumin 130:488–493
15. Matos MG, Pereira PFS, Calefi PS, Ciuffi KJ, Nassar EJ (2009) Preparation of a $GdCaAl_3O_7$ matrix by the non-hydrolytic sol–gel route. J Lumin 129:1120–1124
16. Bhaktha BNS, Kinowski C, Bouazaoui M, Capoen B, Robbe-Cristini O, Beclin F, Roussel P, Ferrari M, Turrell S (2009) Controlled Growth of SnO_2 Nanocrystals in Eu^{3+}-Doped SiO_2–SnO_2 Planar Waveguides: A Spectroscopic Investigation. J Phys Chem C 113:21555–21559
17. Jedlicka SS, Rickus JL, Zemlyanov D (2010) Controllable surface expression of bioactive peptides incorporated into a silica thin film matrix. J Phys Chem C 114:342–344
18. Sanchez C (2010) Advanced nanomaterials: a domain where chemistry, physics and biology meet. CR Chimie 13:1–2
19. Hench LL, West JK (1990) The sol-gel process. Chem Rev 90:33–72
20. Uematsu K, Ochiai A, Toda K, Sato M (2006) Characterization of YVO4:Eu^{3+} phosphors synthesized by microwave heating method. J Alloys Compd 408–412:860–863
21. Wang J, Xua Y, Hojamberdiev M (2009) Hydrothermal synthesis of well-dispersed YVO_4:Eu^{3+} microspheres and their photoluminescence properties. J Alloys Compd 481:896–902
22. Uematsu K, Toda K, Sato M (2005) Characterization of YVO4:Eu^{3+} phosphors synthesized by microwave heating method. J Alloys Compd 389:209–214
23. He F, Yang P, Niu N, Wang W, Gai S, Wang D, Lin J (2010) Hydrothermal synthesis and luminescent properties of YVO4:Ln3 + (Ln = Eu, Dy, and Sm) microspheres. J Colloid Interface Sci 343:71–78
24. Zhou YH, Lin J (2005) Morphology control and luminescence properties of YVO4:Eu phosphors prepared by spray pyrolysis. Opt Mater 27:1426–1432
25. Su X-Q, Yan B (2005) In situ chemical co-precipitation synthesis of YVO_4:RE (RE = Dy^{3+}, Sm^{3+}, Er^{3+}) phosphors by assembling hybrid precursors. J Non-Cryst Solids 351:3542–3546
26. Zhou YH, Lin J (2006) Luminescent properties of YVO_4:Dy^{3+} phosphors prepared by spray pyrolysis. J Alloys Compd 408–412:856–859
27. Chang YS, Huang FM, Tsai YY, Teoh LG (2009) Synthesis and photoluminescent properties of YVO_4:Eu^{3+} nano-crystal phosphor prepared by Pechini process. J Lumin 129:1181–1185
28. Zhang H, Fu X, Niu S, Xin Q (2008) Synthesis and luminescent properties of nanosized YVO4:Ln (Ln = Sm, Dy). J Alloys Compd 457:61–65
29. Li J, Chem Y, Yin Y, Yao F, Yao K (2007) Modulation of nano-hydroxyapatite size via formation on chitosan-gelatin network film in situ. Biomaterials 28:781–790
30. Murakami K (1998) Phosphors and lamps. In Shionoya S, Yen WM (eds) Phosphor handbook. CRC Press.
31. Hsu C, Powell RC (1975) Energy transfer in europium doped yttrium vanadate crystals. J Lumin 10:273–293
32. Blasse G, Grabmaier BC (1994) Luminescent materials. Springer-Verlag, Berlin
33. Yanhong L, Guangyan H (2005) Synthesis and luminescence properties of nanocrystalline YVO_4:Eu^{3+}. J Solid State Chem 178:645–649
34. Nassar EJ, Pereira PFS, Nassor ECO, Avila LR, Ciuffi KJ, Calefi PS (2007) Nonhydrolytic sol-gel synthesis and characterization of YAG. J Mater Sci 42:2244–2249
35. Zhou L, Choy WCH, Shi J, Gong M, Liang H, Yuk TI (2005) Synthesis, vacuum ultraviolet and near ultraviolet-excited luminescent properties of $GdCaAl_3O_7$:RE^{3+} (RE=Eu, Tb). J Solid State Chem 178:3004–3009